

Extreme magnetic field-boosted superconductivity in a high-temperature superconductor

Km Rubi,^{1,*} King Yau Yip,² Elizabeth Krenkel,³ Nurul Fitriyah,²
Xing Gao,² Saurav Prakash,² S. Lin Er Chow,² Tsz Fung Poon,⁴
Mun K. Chan,¹ David Graf,⁵ A. Ariando,^{2,†} and Neil Harrison¹

¹*National High Magnetic Field Laboratory,*

Los Alamos National Laboratory, Los Alamos, NM 87545, USA

²*Department of Physics, National University of Singapore, 117551 Singapore*

³*Center for Integrated Nanotechnologies,*

Los Alamos National Laboratory, Los Alamos, NM 87545, USA

⁴*Department of Physics, The Chinese University of Hong Kong, Shatin, Hong Kong, China*

⁵*National High Magnetic Field Laboratory,*

Florida State University, Tallahassee, Florida 32310, USA

(Dated: August 25, 2025)

Abstract

Magnetic fields typically suppress superconductivity through Pauli and orbital limiting effects. However, there are rare instances of magnetic-field-induced superconductivity, as seen in Chevrel phase compounds [1], organic conductors [2], uranium-based heavy-fermion systems [3, 4], and moiré graphene [5]—though these materials possess inherently low superconducting transition temperatures (T_c). Here, we demonstrate high field-stabilized superconductivity in a class of materials with a significantly higher T_c (up to 40 K): the infinite-layer nickelates [6]. Both low-field and high-field superconducting states can be plausibly explained by a compensation mechanism akin to the Jaccarino–Peter effect. These findings demonstrate the possibility of achieving substantially enhanced upper critical fields in high-temperature superconductors.

There is considerable technological interest in superconducting state that remains robust in high magnetic fields [7–9]. One significant challenge is that strong magnetic fields are typically detrimental to superconductivity. This occurs via two primary mechanisms: Pauli pair breaking [10, 11], where the Zeeman interaction aligns electron spins and disrupts spin-singlet Cooper pairs, and orbital pair breaking, where magnetic flux penetrates the superconductor in the form of vortices, ultimately destroying phase coherence when the vortex density becomes too high [12].

One possible way to circumvent the detrimental effects of magnetic fields on superconductivity is to exploit unusual situations in which the interplay between conduction electrons and magnetism gives rise to magnetic-field-induced superconducting states [1–5, 13]. Magnetic-field-induced superconductivity was first discovered in Chevrel phase compounds [1]. Since then, unconventional field-induced superconducting states have been reported in diverse systems, including the organic conductor λ -(BETS) $_2$ FeCl $_4$ [2, 13], uranium-based compounds such as URhGe [3] and UTe $_2$ [4, 14, 15], and twisted trilayer graphene [5]. However, a common limitation of all known field-induced superconducting states is that they occur in materials with intrinsically low superconducting transition temperatures (T_c). This is often attributed to factors such as conventional electron–phonon-mediated pairing [1] or the

* email: rubi@lanl.gov

† email: ariando@nus.edu.sg

presence of narrow electronic bandwidths [3–5], which enhance electronic correlations but typically suppress T_c .

Here we demonstrate that infinite-layer nickelates [6, 16–18] provide a compelling example of a magnetic-field-induced superconducting state occurring in a material that also hosts high-temperature superconductivity, comparable to that of the cuprates [19]. Specifically, we observe this phenomenon in SmNiO_2 thin films, where Sm is partially substituted with Eu, Ca, and Sr—a system referred to as (SECS) NiO_2 [6]. We find field-induced superconductivity to be most clearly demonstrated in a sample with a transition temperature of $T_c \approx 12$ K and extreme field-boosted superconductivity in samples with $T_c \approx 22$ K and 32 K. Notably, by carefully tuning hole-dopants Eu, Ca, and Sr, the superconductivity in (SECS) NiO_2 is achieved up to 40 K [6]. This raises the possibility of realizing field-stabilized superconducting state in unprecedented high magnetic fields.

Figure 1 shows magnetoresistance curves of (SECS) NiO_2 ($T_c = 11.7$ K) as a function of magnetic field (H) at different temperatures (T), with H aligned along the crystalline c -axis (Fig. 1A), and as a function of the inclination angle θ at fixed temperature ($T = 1.8$ K), where H is tilted away from the c -axis toward the in-plane a -axis direction (Fig. 1B). Salient features of the data in Fig. 1 include an initial sharp transition from a superconducting state to a resistive state at $H \approx 1$ T (accompanied by an additional dip at $H \approx 2$ T for $T < 1.5$ K), followed by a broad minimum in the resistivity centred on $H \approx 15$ T, that shifts progressively to higher magnetic fields at higher angles. At sufficiently high magnetic fields, the resistivity increases and saturates at a near constant value consistent with reaching the normal state.

As shown in Fig. 1 and Extended Data Fig. 1, a magnetic-field-induced re-entrant superconducting state is evidenced by the vanishing electrical resistivity at temperatures at $T \approx 0.35$ K at $\theta = 0^\circ$, and at angles above $\theta = 65^\circ$ (26°) at $T = 1.8$ K (0.6 K). In the re-entrant superconducting state, the resistivity drops by four orders of magnitude, as demonstrated in the log-scale plot in Extended Data Fig. 2. Figure 2 shows a phase diagram constructed from the data in Figs. 1 and extended data Fig. 3. Here T_c and H_{c2} are defined as the midpoint of the resistive transition, at which the resistivity is halfway between zero and its saturated normal-state value. The $T - H$ phase diagram (Fig. 2A) clearly reveals two distinct superconducting phases: (1) a low-field superconducting state and (2) a high-field-induced reentrant superconducting state. These two phases merge as the direction of H is rotated toward the in-plane a -axis, with superconductivity persisting up to 60 T (52

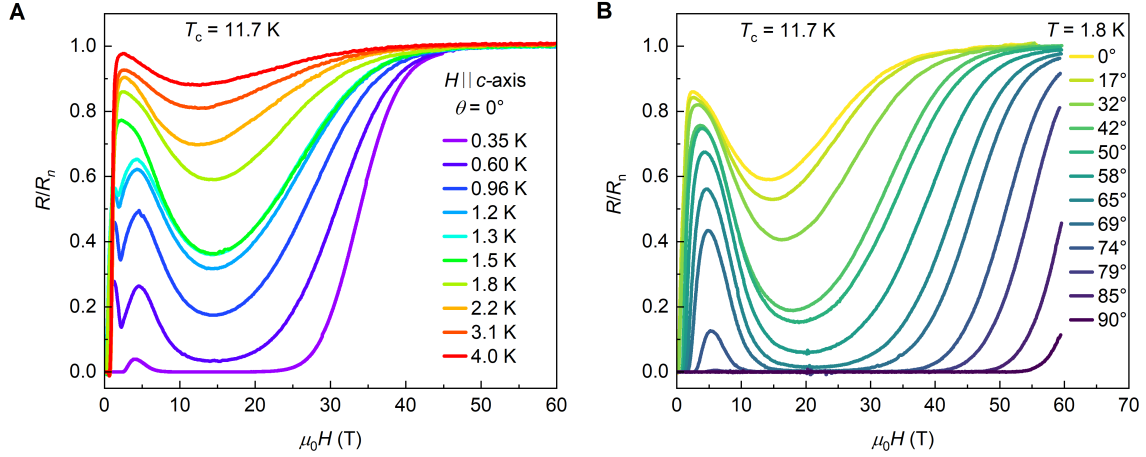


FIG. 1. **Re-entrant superconductivity at high magnetic fields in a (SECS)NiO₂ superconductor ($T_c = 11.7$ K).** (A) Measured electrical resistance R normalised with the resistance in normal state (R_n) versus magnetic field H at different temperatures as indicated for H applied along c axis. (B) Normalised resistance R/R_n at different field orientations θ , at a temperature of $T = 1.8$ K. Inset in A is the schematic of H alignment, moving away from the out-of-plane c -axis ($\theta = 0^\circ$) toward the in-plane a -axis ($\theta = 90^\circ$).

T) at $T = 0.6$ K (1.8 K).

The mechanisms underlying reentrant superconductivity have been the subject of extensive debate. Proposed explanations include compensation of the applied field by an internal exchange field [1, 13, 14], electron pairing mediated by spin fluctuations [3, 20, 21], field-enhanced spin reorientation or spin-triplet pairing [3, 4], field-induced magnetic transitions and Fermi-surface reconstructions [22], and Landau-level broadening near the quantum limit [23]. Given the presence of rare-earth elements Sm and Eu, it is plausible that field-induced reentrant superconductivity in (SECS)NiO₂ arises from a significant exchange interaction between the conduction electrons and localized rare-earth magnetic moments [24]. In magnetic ion-doped superconductors (e.g., Eu-doped chalcogenides [1, 25] and Fe-based organic conductors [2, 13]), the conduction electrons experience an internal exchange field from magnetic ions. If the internal field aligns opposite to the applied magnetic field direction, the two can partially or completely cancel each other, reducing the pair-breaking effect of the external field and allowing superconductivity to reappear at high fields. This magnetic-field compensation mechanism is known as the Jaccarino-Peter effect [24]. In the case of

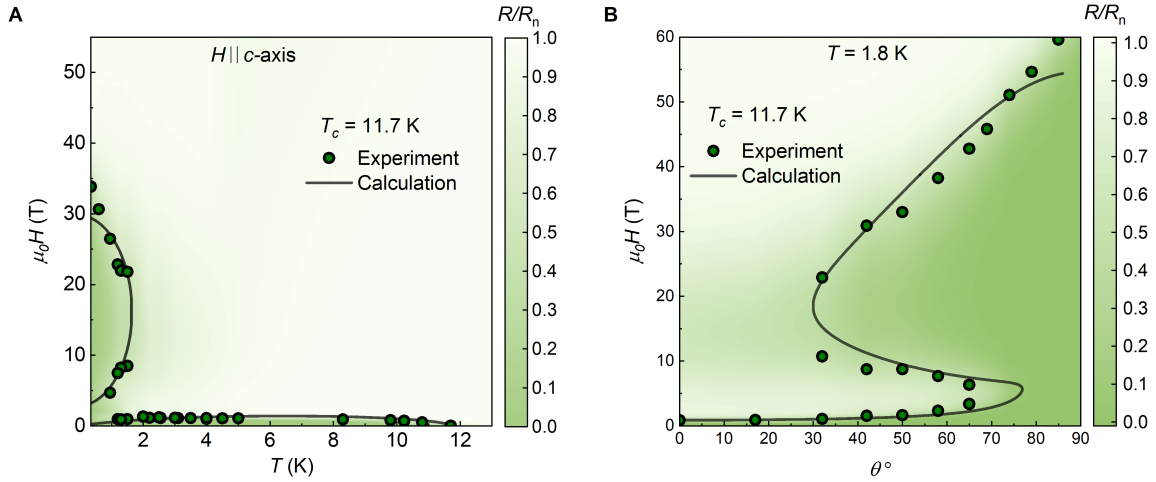


FIG. 2. **Phase diagrams and evolution of upper critical field with temperature and tilt angle of (SECS)NiO₂ ($T_c = 11.7$ K).** Phase diagrams (A) temperature versus magnetic fields when the field applied along c-axis and (B) tilt angle versus magnetic fields at a fixed temperature of 1.8 K. Symbols represent experimentally determined upper critical fields H_{c2} , while solid lines show calculated H_{c2} based on the WHH model. H_{c2} is defined as the midpoint of the resistive transition, at which the resistivity is 50% of its normal-state value. Two distinct superconducting (SC) phases are observed, which can be tuned by changing the orientation of the magnetic field relative to the sample.

(SECS)NiO₂, we find that the essential features of the phase diagrams in Fig. 2 are well captured by a modified Werthamer–Helfand–Hohenberg (WHH) model [26] for the superconducting critical field, adapted to include the effects of an exchange splitting field H_J (see Methods). Moreover, the results of some experiments on the recently highlighted reentrant superconductor UTe₂ have suggested that the Jaccarino–Peter effect may be responsible for reentrant superconductivity in this material [14], although alternative mechanism—such as spin-triplet pairing enhanced by magnetic fluctuations [4] or metamagnetic criticality accompanied by Fermi-surface reconstruction [22]—have also been proposed. These effects are less likely to be relevant in (SECS)NiO₂ due to the more localized nature of the f -electrons.

In (SECS)NiO₂, the rare-earth ions in the spacer layers of nickelates are generally believed to adopt the *trivalent* (3+) oxidation state [27]. Since Eu³⁺ has a $J = 0$ nonmagnetic ground state, and Sm³⁺ has a $J = \frac{5}{2}$ ground state but a small Landé g -factor, it seems un-

likely that either ion alone could generate the large exchange field ($H_J \approx -70.5$ T) inferred from our WHH modeling of the critical field in (SECS)NiO₂. However, the oxygen reduction process used to synthesize the nickelates has been shown to significantly lower the valence of Eu, resulting in an intermediate valence state of approximately +2.4 [28]. The large effective moment ($\mu_{\text{eff}} \approx 7\mu_B$ due to the half-filled 4*f* shell of Eu²⁺) needed to account for the lower critical field of ≈ 1 T in (SECS)NiO₂ is consistent with the presence of a significant population of Eu²⁺ ions, which could plausibly give rise to the required exchange field. Interestingly, both the overall structure of the resistivity data and the resulting phase diagram of (SECS)NiO₂ show a striking resemblance to magnetic-field-induced re-entrant superconductivity first reported in the Eu-based chalcogenides such as Eu_{0.75}Sn_{0.25}Mo₆S_{7.2}Se_{0.8} [1, 29].

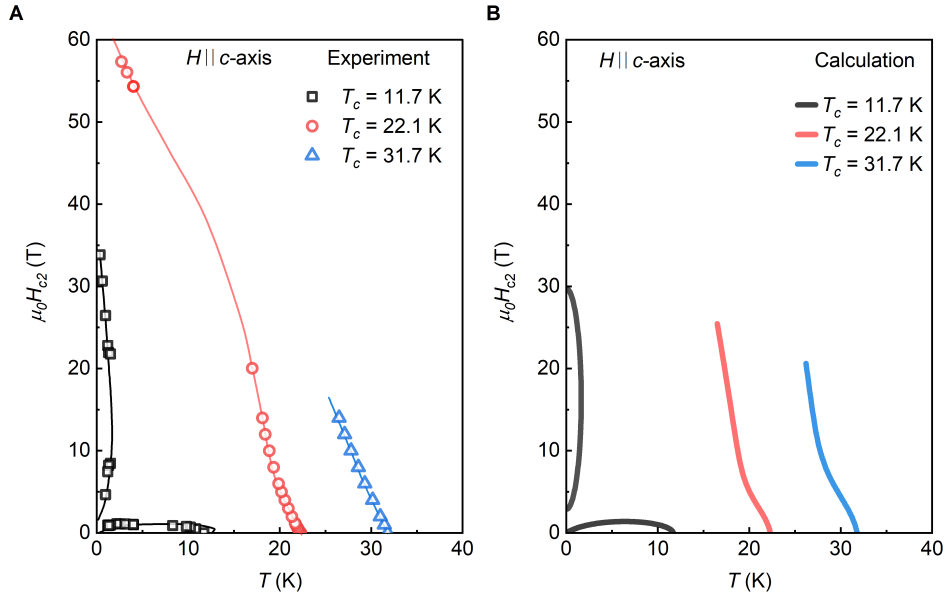


FIG. 3. **Comparison of experimentally obtained and theoretically calculated upper critical fields for three (SECS)NiO₂ samples with different T_c for $H \parallel c$ axis.** (A) Experimental data and (B) theoretical calculations for samples with $T_c = 11.7$ K, 22.1 K, and 31.7 K. Solid lines in (A) are guides to the eye. The sample with $T_c = 11.7$ K exhibits two distinct superconducting (SC) phases, while the higher- T_c samples show only a single SC phase. For higher- T_c SECS, the upper critical field displays a kink followed by a sharp increase with decreasing temperature, without saturation up to 60 T.

The high magnetic-field phase diagram of a reentrant superconductor is sensitive to the

interplay between the Pauli critical field H_P , the orbital critical field H_{c2}^{orb} , and the exchange field (H_J), as well as other factors such as the degree of spin-orbit scattering [29]. For samples with relatively low transition temperatures ($T_c \approx 12$ K in the present case), there is a clear separation between the low-field superconducting state and the magnetic-field-induced superconducting state. However, as T_c increases and the superconducting state becomes more robust (see Extended Data Fig 3), these phases tend to merge, as shown in Extended Data Fig 4, and 5. In such cases, the transition from the low-field superconducting state to the high-field-induced superconducting state is indicated by a subtle kink in the phase boundary. Indeed, for the sample with an intermediate transition temperature ($T_c \approx 22$ K), this kink is directly observable in the experimental data (Fig. 3). For the sample with the highest transition temperature studied here ($T_c \approx 32$ K), the kink is less evident; instead, the phase boundary displays noticeable upward curvature and the superconductivity persists at least up to 65 T. This upward curvature and robust high-field superconductivity provide clear evidence that the exchange field continues to significantly enhance robustness of the high-field superconducting state in samples with higher T_c .

Given the strong experimental evidence for magnetic-field-induced and enhanced superconductivity in (SECS)NiO₂, a key question arises: why have similar phenomena not been clearly observed in other high-temperature superconductors, such as the iron-based pnictides or cuprates? One possible reason could be the strong propensity for magnetic ordering in those materials. For instance, the iron-pnictide superconductor EuFe₂(As_{1-x}P_x)₂ exhibits superconducting transition temperatures T_c in the range of 20 to 30 K when tuned by chemical substitution or pressure [30]. However, it also displays pronounced antiferromagnetic and spin-glass phases involving the Eu magnetic moments, complicating the coexistence of superconductivity and exchange-driven enhancement. Similarly, the cuprate La_{1.8-x}Eu_{0.2}Sr_xCuO₄ (Eu-LSCO), which has $T_c \approx 20$ K, exhibits strong magnetic and charge-ordered stripe phases, with Eu ions playing an active role [31]. In contrast, infinite-layer nickelates, including (SECS)NiO₂, have not yet been reported to exhibit long-range magnetic ordering [32, 33], making them potentially more favorable hosts for exchange-field-enhanced superconductivity.

Another distinguishing factor between the nickelates and other high-temperature superconductors is the significant contribution of the rare-earth 5*d* electrons to the conduction bands, a feature largely absent in the cuprates and iron pnictides [34]. This involvement

of 5d electrons leads to the formation of additional three-dimensional sections of the Fermi surface, which not only alters the electronic structure—potentially suppressing magnetic order—but also greatly enhances the spatial overlap between conduction electrons and localized rare-earth moments. In (SECS)NiO₂, this increased overlap may explain the large magnitude of the exchange field ($H_J \approx -70.5$ T) required by the modified WHH model.

In summary, we have discovered extreme field-reentrant superconductivity in an infinite-layer nickelate system, Sm_{1-x-y-z}Eu_xCa_ySr_zNiO₂, referred to as (SECS)NiO₂. Unlike previously known reentrant superconductors, which typically exhibit low critical temperatures ($T_c < 4$ K) [1–5], (SECS)NiO₂ displays superconductivity with T_c values reaching up to 40 K at ambient pressure [6]. Our measurements on three (SECS)NiO₂ samples with varying T_c reveal extraordinarily large upper critical fields. Notably, the $T_c \approx 12$ K sample exhibits a clear separation between the low-field superconducting state and a high-field-induced reentrant superconducting phase, consistent with a Jaccarino–Peter compensation mechanism. Remarkably, the upper critical field reaches 35 T for $T_c \approx 12$ K, 58 T for $T_c \approx 22$ K, and greatly exceeds 65 T for $T_c \approx 32$ K when the magnetic field is applied along the c -axis (Fig. 3 and Extended data Fig. 5). Not even the onset of resistive transition is seen up to 65 T at 1.5 K for $T_c \approx 32$ K. Our findings highlight the technological potential of nickelates for ultra high magnetic field applications such as superconducting magnets and quantum magnetometers.

-
- [1] H. W. Meul, C. Rossel, M. Decroux, O. Fischer, G. Remenyi, and A. Briggs, [Physical Review Letters](#) **53**, 497 (1984), published 30 July 1984.
 - [2] S. Uji, H. Shinagawa, T. Terashima, T. Yakabe, Y. Terai, M. Tokumoto, A. Kobayashi, H. Tanaka, and H. Kobayashi, [Nature](#) **410**, 908 (2001).
 - [3] F. Lévy, I. Sheikin, B. Grenier, and A. D. Huxley, [Science](#) **309**, 1343 (2005).
 - [4] S. Ran, C. Eckberg, Q.-P. Ding, Y. Furukawa, T. Metz, S. R. Saha, I.-L. Liu, M. Zic, H. Kim, J. Paglione, *et al.*, [Science](#) **365**, 684 (2019).
 - [5] Y. Cao, J. M. Park, K. Watanabe, T. Taniguchi, and P. Jarillo-Herrero, [Nature](#) **595**, 526 (2021).
 - [6] S. L. E. Chow, Z. Luo, and A. Ariando, [Nature](#) **642**, 58 (2025).

- [7] D. Uglietti, [Superconductor Science and Technology](#) **32**, 053001 (2019), indexed April 22, 2019.
- [8] N. Mitchell, J. Zheng, C. Vorpahl, V. Corato, C. Sanabria, M. Segal, B. Sorbom, R. Slade, G. Brittles, R. Bateman, Y. Miyoshi, N. Banno, K. Saito, A. Kario, H. T. Kate, P. Bruzzone, R. Wesche, T. Schild, N. Bykovskiy, A. Dudarev, M. Mentink, F. J. Mangiarotti, K. Sedlak, D. Evans, D. C. V. D. Laan, J. D. Weiss, M. Liao, and G. Liu, [Superconductor Science and Technology](#) **34**, 103001 (2021).
- [9] V. Shiltsev and F. Zimmermann, [Reviews of Modern Physics](#) **93**, 015006 (2021), indexed April 19, 2021.
- [10] A. M. Clogston, [Physical Review Letters](#) **9**, 266 (1962), published 15 September 1962.
- [11] B. S. Chandrasekhar, [Applied Physics Letters](#) **1**, 7 (1962), aPL Classic Papers Collection.
- [12] M. Tinkham, *Introduction to Superconductivity*, 2nd ed. (Dover Publications, Mineola, New York, 2004).
- [13] L. Balicas, J. Brooks, K. Storr, S. Uji, M. Tokumoto, H. Tanaka, H. Kobayashi, A. Kobayashi, V. Barzykin, and L. Gor’Kov, *Physical review letters* **87**, 067002 (2001).
- [14] T. Helm, M. Kimata, K. Sudo, A. Miyata, J. Stirnat, T. Förster, J. Hornung, M. König, I. Sheikin, A. Pourret, *et al.*, *Nature Communications* **15**, 37 (2024).
- [15] S. K. Lewin, P. Czajka, C. E. Frank, G. Saucedo Salas, G. T. Noe II, H. Yoon, Y. S. Eo, J. Paglione, A. H. Nevidomskyy, J. Singleton, *et al.*, *Science* **389**, 512 (2025).
- [16] D. Li, K. Lee, B. Y. Wang, M. Osada, S. Crossley, H. R. Lee, Y. Cui, Y. Hikita, and H. Y. Hwang, [Nature](#) **572**, 624 (2019).
- [17] H. Sun, M. Huo, X. Hu, J. Li, Z. Liu, Y. Han, L. Tang, Z. Mao, P. Yang, B. Wang, J. Cheng, D.-X. Yao, G.-M. Zhang, and M. Wang, [Nature](#) **621**, 493 (2023).
- [18] G. Zhou, W. Lv, H. Wang, Z. Nie, Y. Chen, Y. Li, H. Huang, W.-Q. Chen, Y.-J. Sun, Q.-K. Xue, and Z. Chen, [Nature](#) **640**, 641 (2025).
- [19] B. Keimer, S. A. Kivelson, M. R. Norman, S. Uchida, and J. Zaanen, [Nature](#) **518**, 179 (2015).
- [20] D. Aoki, A. Huxley, E. Ressouche, D. Braithwaite, J. Flouquet, J.-P. Brison, E. Lhotel, and C. Paulsen, *Nature* **413**, 613 (2001).
- [21] N. T. Huy, A. Gasparini, D. E. de Nijs, Y. Huang, J. C. P. Klaasse, T. Gortenmulder, A. de Visser, A. Hamann, T. Görlach, and H. v. Löhneysen, [Phys. Rev. Lett.](#) **99**, 067006 (2007).

- [22] Z. Wu, T. I. Weinberger, A. J. Hickey, D. V. Chichinadze, D. Shaffer, A. Cabala, H. Chen, M. Long, T. J. Brumm, W. Xie, Y. Ling, Z. Zhu, Y. Skourski, D. E. Graf, V. Sechovský, M. Vališka, G. G. Lonzarich, F. M. Grosche, and A. G. Eaton, [Phys. Rev. X **15**, 021019 \(2025\)](#).
- [23] M. Rasolt and Z. Teshanović, [Rev. Mod. Phys. **64**, 709 \(1992\)](#).
- [24] V. Jaccarino and M. Peter, [Physical Review Letters **9**, 290 \(1962\)](#), indexed January 1, 1962.
- [25] O. Fischer, M. Decroux, S. Roth, R. Chevrel, and M. Sergent, Journal of Physics C: Solid State Physics **8**, L474 (1975).
- [26] N. R. Werthamer, E. Helfand, and P. C. Hohenberg, [Physical Review **147**, 295 \(1966\)](#), published 8 July 1966.
- [27] Y. Ji, J. Liu, L. Li, and Z. Liao, [Journal of Applied Physics **130**, 060901 \(2021\)](#).
- [28] W. Wei, D. Vu, Z. Zhang, F. J. Walker, and C. H. Ahn, [Science Advances **9**, eadh3327 \(2023\)](#).
- [29] C. Rossel, H. W. Meul, M. Decroux, O. Fischer, G. Remenyi, and A. Briggs, [Journal of Applied Physics **57**, 3099 \(1985\)](#).
- [30] S. Zapf, H. S. Jeevan, T. Ivek, F. Pfister, F. Klingert, S. Jiang, D. Wu, P. Gegenwart, R. K. Kremer, and M. Dressel, [Physical Review Letters **110**, 237002 \(2013\)](#).
- [31] F. Laliberté, J. Chang, N. Doiron-Leyraud, E. Hassinger, R. Daou, M. Rondeau, B. J. Ramshaw, R. Liang, D. A. Bonn, W. N. Hardy, S. Pyon, T. Takayama, H. Takagi, I. Sheikin, L. Malone, C. Proust, K. Behnia, and L. Taillefer, [Nature Communications **2**, 432 \(2011\)](#).
- [32] J. Fowlie, M. Hadjimichael, M. M. Martins, D. Li, M. Osada, B. Y. Wang, K. Lee, Y. Lee, Z. Salman, T. Prokscha, *et al.*, Nature Physics **18**, 1043 (2022).
- [33] Y. Yan, Y. Chan, X. Hong, S. Chow, Z. Luo, Y. Li, T. Wang, Y. Wu, I. Biało, N. Fitriyah, *et al.*, arXiv preprint arXiv:2507.18373 (2025).
- [34] Y. Nomura and R. Arita, [Reports on Progress in Physics **85**, 052501 \(2022\)](#), published 28 March 2022.
- [35] B. Y. Wang, D. Li, B. H. Goodge, K. Lee, M. Osada, S. P. Harvey, L. F. Kourkoutis, M. R. Beasley, and H. Y. Hwang, Nature Physics **17**, 473 (2021).
- [36] B. Y. Wang, T. C. Wang, Y.-T. Hsu, M. Osada, K. Lee, C. Jia, C. Duffy, D. Li, J. Fowlie, M. R. Beasley, *et al.*, Science advances **9**, eadf6655 (2023).
- [37] A. P. Mackenzie, S. Julian, G. Lonzarich, A. Carrington, S. Hughes, R. Liu, and D. Sinclair, Physical review letters **71**, 1238 (1993).

- [38] Y.-T. Hsu, M. Hartstein, A. J. Davies, A. J. Hickey, M. K. Chan, J. Porras, T. Loew, S. V. Taylor, H. Liu, A. G. Eaton, *et al.*, Proceedings of the National Academy of Sciences **118**, e2021216118 (2021).
- [39] Y. Yu and S. Kivelson, Physical Review B **99**, 144513 (2019).
- [40] A. Gurevich, Physical Review B—Condensed Matter and Materials Physics **82**, 184504 (2010).

I. METHODS

Sample Growth and characterization

The infinite-layer nickelates $\text{Sm}_{1-x-y-z}\text{Eu}_x\text{Ca}_y\text{Sr}_z\text{NiO}_2$ thin films (thickness $\approx 5\text{-}8$ nm) were synthesized on NdGaO_3 (110) substrates following the method described in [6]. The x-ray diffraction and scanning transmission electron microscopy techniques were used to assess quality of thin films. See details of growth process and characterization in [6]. The sample compositions are given in Table 1.

Transport measurements

Samples were wire bonded using ultrasonic wire bonder for electrical transport measurements. High-field transport measurements were performed at both the DC and pulsed-field facilities of the National High Magnetic Field Laboratory. Pulsed-field measurements were conducted using a 60 T resistive magnet with a pulse duration of ~ 500 ms and a 70 T Duplex magnet with a pulse duration of ~ 60 ms. To minimize eddy current heating during these measurements, we used samples of size $\sim 0.5 \times 0.5$ mm² and adopted the van der Pauw method. Measurements above 4 K were done in helium-4 gas. Measurements between 4 K and 1.5 K were conducted by immersing the samples in liquid helium-4, while those below 1.5 K were performed in liquid helium-3. For temperatures below 0.5 K, measurements were carried out in high DC fields using a 45 T hybrid magnet. Additional measurements in DC magnetic fields up to 14 T were performed using a Physical Property Measurement System (PPMS) from Quantum Design Inc. A standard lock-in technique was used for all transport measurements. Home-made rotators were used for in-situ rotation of samples in magnetic fields.

Theoretical model

We employ the Werthamer–Helfand–Hohenberg (WHH) model [26], a microscopic theory that describes the upper critical magnetic field of conventional type-II superconductors in

the dirty limit, incorporating the influence of localized magnetic impurities to both orbital and paramagnetic pair-breaking effects and to spin-orbit scattering. The implicit equation we used to fit experimental H_{c2} as a function of temperature (Fig. 2A) is [26, 29]

$$\ln \frac{1}{t} = \left(\frac{1}{2} + \frac{i(\lambda_{\text{so}} - \lambda_m)}{4\gamma} \right) \times \psi \left(\frac{1}{2} + \frac{h + \lambda_m + \frac{1}{2}(\lambda_{\text{so}} - \lambda_m) + i\lambda}{2t} \right) + \left(\frac{1}{2} - \frac{i(\lambda_{\text{so}} - \lambda_m)}{4\gamma} \right) \times \psi \left(\frac{1}{2} + \frac{h + \lambda_m + \frac{1}{2}(\lambda_{\text{so}} - \lambda_m) - i\lambda}{2t} \right) - \psi \left(\frac{1}{2} \right) \quad (1)$$

where $\lambda = [\alpha^2(h + h_J)^2 - \frac{1}{4}(\lambda_{\text{so}} - \lambda_m)^2]^{1/2}$. The parameters formulated in reduced units are: $t = \frac{T}{T_c}$, $h = 0.281 \frac{H_{c2}(T)}{H_{c2}^{\text{orb}}(0)}$, and $h_J = 0.281 \frac{H_J(T)}{H_{c2}^{\text{orb}}(0)}$, where T_c is the critical SC transition temperature, $H_{c2}^{\text{orb}}(0)$ is the orbital-limited critical field at absolute zero temperature, and H_J is the exchange field described by a Brillouin function with $J = 7/2$ for Eu^{2+} ions. λ_{so} and λ_m are the spin-orbit and magnetic scattering parameters, respectively. ψ is the digamma function and α is the Maki parameter given by $\alpha = \sqrt{2} \frac{H_{c2}^{\text{orb}}(0)}{H_P}$ with H_P being the Pauli-limited critical field. Assuming $\lambda_m = 0$ and using only three fitting parameters λ_{so} , α , and H_J (listed in Table 1) – we can produce the key features of the experimental data, including low-field and high-field superconducting states, as shown in Fig. 2A and Fig. 3B. However, the steep increase in H_{c2} below 0.6 K remains unexplained using simplified WHH model and, therefore, needs elaborate theory efforts that is beyond the scope of this work. Notably, low-temperature non-saturating H_{c2} has also been reported in other nickelates [35, 36] and cuprates [37, 38] and various mechanisms, including an interplay between superconductivity and a density wave [39] and the existence of multiple bands [40], are proposed to account for this phenomenon.

Samples		H_{c2}^{orb}	λ_{so}	α	H_J
$T_c = 11.7$ K	$\text{Sm}_{0.53}\text{Eu}_{0.4}\text{Ca}_{0.07}\text{NiO}_2$	45 T	35	7.3	- 70.5 T
$T_c = 22.1$ K	$\text{Sm}_{0.77}\text{Eu}_{0.12}\text{Ca}_{0.04}\text{Sr}_{0.05}\text{NiO}_2$	85.8 T	65	7.3	-70.5 T
$T_c = 32.7$ K	$\text{Sm}_{0.73}\text{Eu}_{0.2}\text{Ca}_{0.07}\text{NiO}_2$	122.3 T	30	7.3	-70.5 T

TABLE I. H_{c2}^{orb} and fitting parameters for temperature-dependent H_{c2} for (SECS)NiO₂.

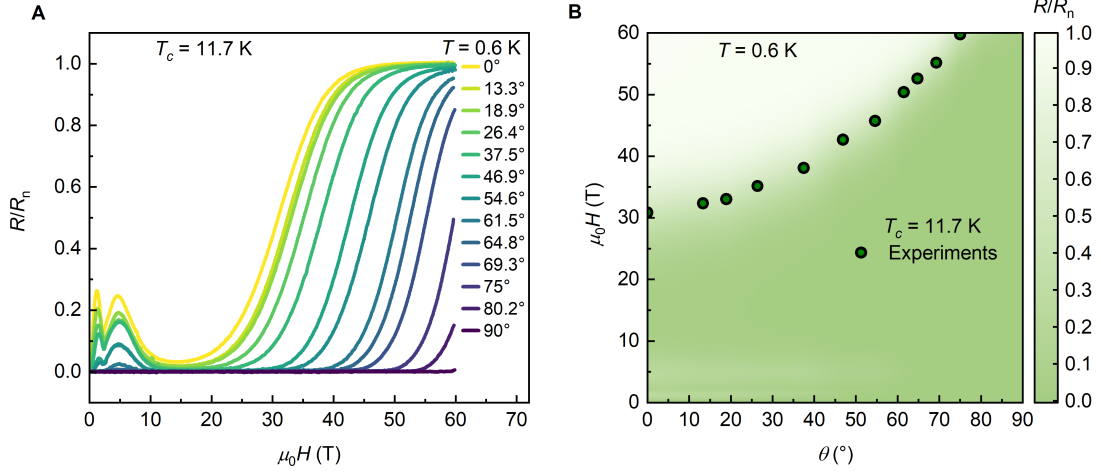
For angular dependence of upper critical field (Fig. 2B), we used the equation

$$H_{c2}(\theta) = \frac{H_{c2,\parallel}^{\text{orb}}}{\sqrt{\cos^2\theta + \gamma^{-2}\sin^2\theta + \eta\gamma^{-2}\sin^2\theta\cos^2\theta}} \quad (2)$$

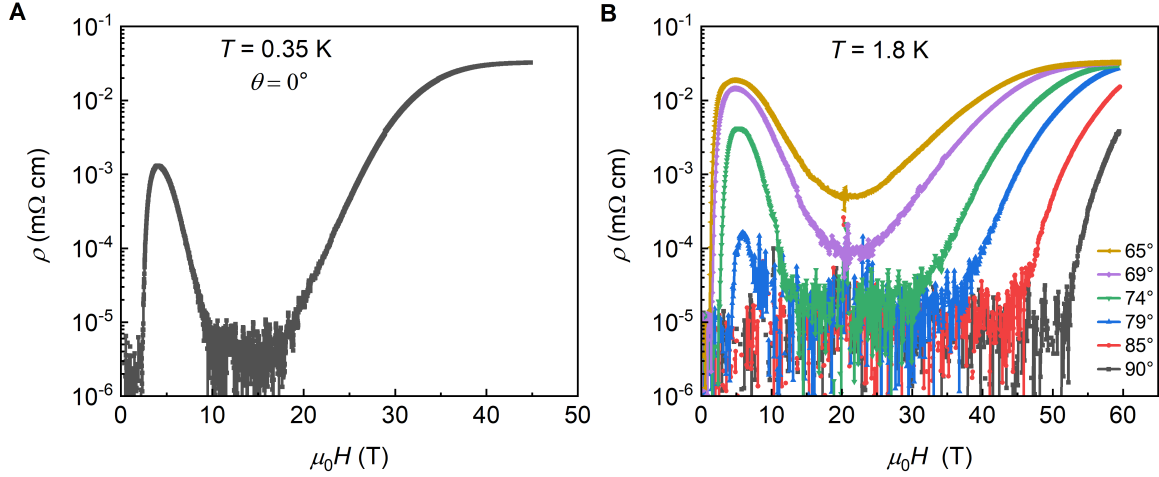
where $H_{c2,\parallel}^{\text{orb}}$ is the orbital H_{c2} in the field parallel to a -axis. The fitting parameters are $H_{c2,\parallel}^{\text{orb}} = 75$ T, $\gamma = 1.36$, and $\eta = 0.3$.

Acknowledgements This work was performed as part of the Department of Energy (DoE) BES project ‘Science of 100 tesla.’ The National High Magnetic Field Laboratory is funded by the National Science Foundation through NSF/DMR-2128556, the State of Florida and DoE. We acknowledge the support from the Ministry of Education (MOE), Singapore, under its Tier-2 Academic Research Fund (AcRF), Grant No. MOE-T2EP50123-0013, the SUSTech-NUS Joint Research Program, and by the MOE Tier-3 Grant (MOE-MOET32023-0003) ‘Quantum Geometric Advantage’.

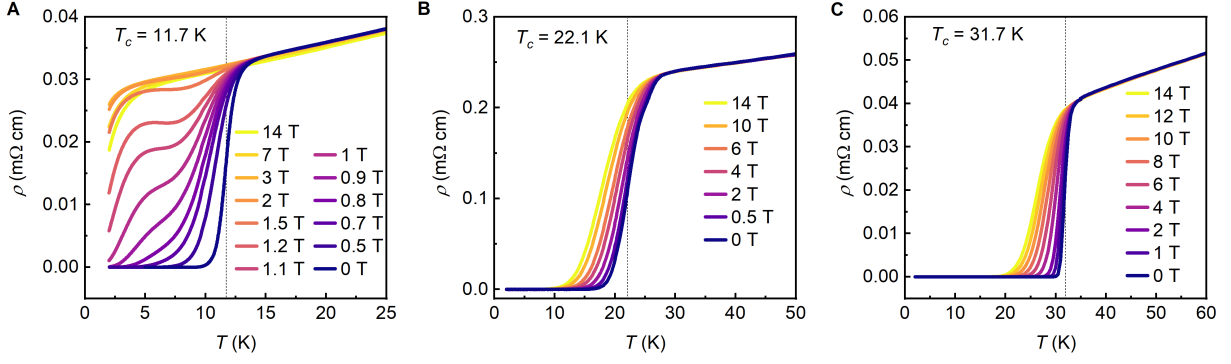
Author contributions KR, KYY, AA, and NH conceived and designed the project. NF, GX, SP, and SLEC grew nickelate thin films under the guidance of AA. KR, EK, and MKC conducted transport measurements in high pulsed magnetic fields. KR, KYY and DG performed measurements in high dc magnetic fields. KR measured in moderate fields in PPMS. NH performed theoretical calculations. KR and NH analyzed the data and wrote the manuscript with input from all authors.



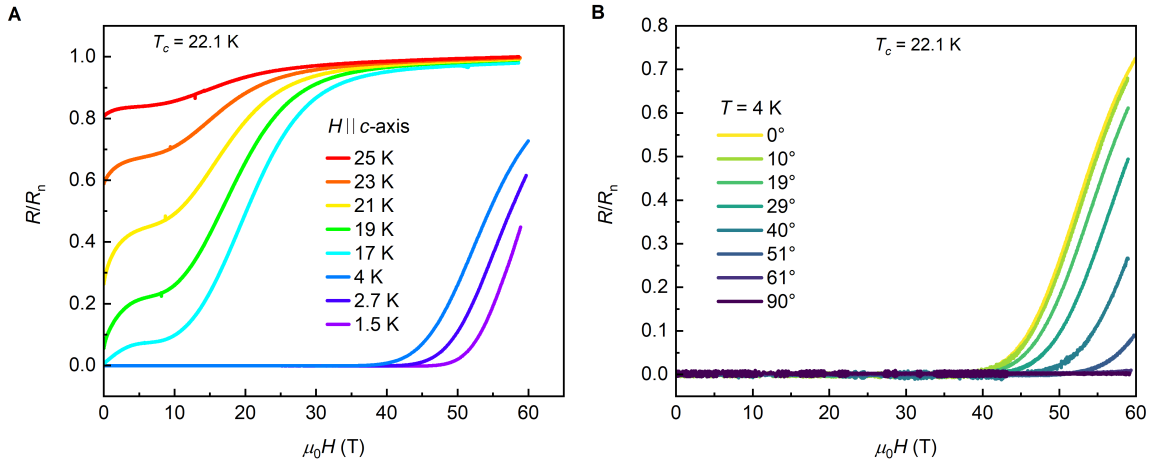
Extended Data Fig. 1. **Angular dependence of re-entrant superconductivity at 0.6 K for (SECS)NiO₂ with $T_c = 11.7$ K.** (A) Normalised resistance as a function of field at different tilt angles, and (B) Colour contour plot of the data with upper critical field values.



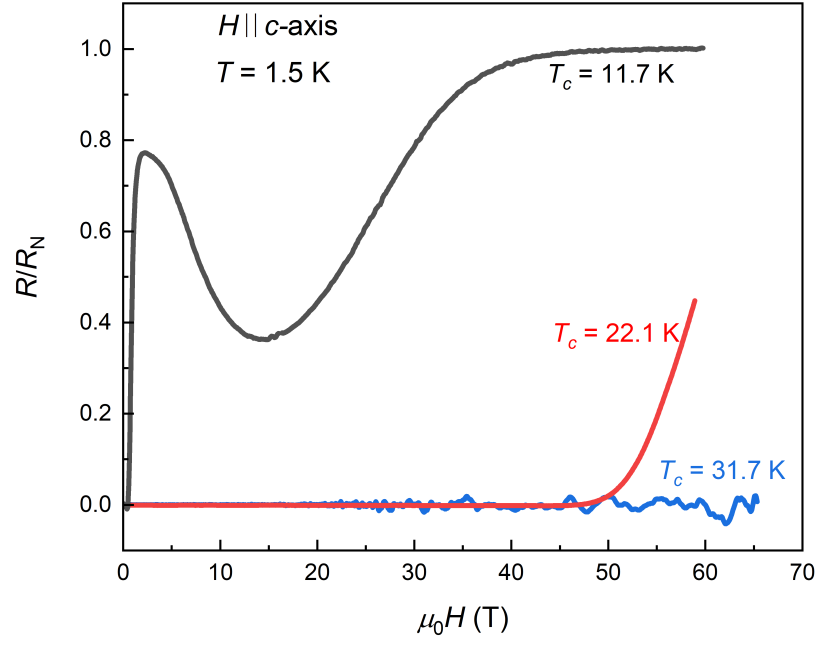
Extended Data Fig. 2. **Log-scale resistivity of (SECS)NiO₂ with $T_c = 11.7$ K.** (A) Resistivity vs field at 0.35 K for 0° and (B) at 1.8 K for various inclination angles above 65° . The resistivity value drops by four orders of magnitude as the sample transitions from the normal to the superconductive state..



Extended Data Fig. 3. **Comparison of resistivity of three (SECS)NiO₂ samples with different T_c .** Temperature dependence of resistivity for samples (a) $T_c = 11.7$ K, (b) $T_c = 22.1$ K, and (c) $T_c = 31.7$ K measured at various magnetic field values.



Extended Data Fig. 4. **High-field robust superconductivity in (SECS)NiO₂ with $T_c = 22.1$ K.** (A) Normalised resistance as a function of field at different (A) temperatures for $H \parallel c$ axis, and (B) for different tilt angles at $T = 4$ K.



Extended Data Fig. 5. **Comparison of field-induced superconductivity in (SECS)NiO₂ with different T_c for $H \parallel c$ axis.** (SECS)NiO₂ with $T_c = 31.7$ K persists superconductivity up to 65 T.